J Neurophysiol 118: 3282–3292, 2017.
First published September 20, 2017; doi:10.1152/jn.00172.2017.

RESEARCH ARTICLE | *The Mouse Visual System*

Nonuniform surround suppression of visual responses in mouse V1

Jason M. Samonds,[1,2] Berquin D. Feese,[1,3] Tai Sing Lee,[1,2] and Sandra J. Kuhlman[1,3]
[1]*Center for the Neural Basis of Cognition, Carnegie Mellon University, Pittsburgh, Pennsylvania;* [2]*Computer Science Department, Carnegie Mellon University, Pittsburgh, Pennsylvania; and* [3]*Department of Biological Sciences, Carnegie Mellon University, Pittsburgh, Pennsylvania*

Submitted 9 March 2017; accepted in final form 14 September 2017

Samonds JM, Feese BD, Lee TS, Kuhlman SJ. Nonuniform surround suppression of visual responses in mouse V1. *J Neurophysiol* 118: 3282–3292, 2017. First published September 20, 2017; doi:10.1152/jn.00172.2017.—Complex receptive field characteristics, distributed across a population of neurons, are thought to be critical for solving perceptual inference problems that arise during motion and image segmentation. For example, in a class of neurons referred to as "end-stopped," increasing the length of stimuli outside of the bar-responsive region into the surround suppresses responsiveness. It is unknown whether these properties exist for receptive field surrounds in the mouse. We examined surround modulation in layer 2/3 neurons of the primary visual cortex in mice using two-photon calcium imaging. We found that surround suppression was significantly asymmetric in 17% of the visually responsive neurons examined. Furthermore, the magnitude of asymmetry was correlated with orientation selectivity. Our results demonstrate that neurons in mouse primary visual cortex are differentially sensitive to the addition of elements in the surround and that individual neurons can be described as being either uniformly suppressed by the surround, end-stopped, or side-stopped.

NEW & NOTEWORTHY Perception of visual scenes requires active integration of both local and global features to successfully segment objects from the background. Although the underlying circuitry and development of perceptual inference is not well understood, converging evidence indicates that asymmetry and diversity in surround modulation are likely fundamental for these computations. We determined that these key features are present in the mouse. Our results support the mouse as a model to explore the neural basis and development of surround modulation as it relates to perceptual inference.

primary visual cortex; mouse; vision; surround; orientation; receptive field

INTRODUCTION

Neurons throughout the visual system in several species exhibit surround suppression, where stimuli displayed outside of the classical receptive field generally decrease the response to stimuli displayed within the classical receptive field even though when the surround stimuli are displayed alone, they do not elicit a response (Allman et al. 1985; Cavanaugh et al. 2002a, 2002b; Guo et al. 2005; Jones et al. 2001; Knierim and van Essen 1992; Sceniak et al. 1999). Recent advances in genetically identifying cell types and targeted optogenetic activation of these various cell types in mice has helped to begin to reveal the specific circuitry that underlies this phenomenon (Adesnik et al. 2012; Nienborg et al. 2013; Self et al. 2014). For some neurons in the visual cortex in higher species, the surround can exert a more complex effect. Stimuli in the surround suppress the response to the center stimulus only when presented in particular regions, such as at the ends (Dreher 1972; Gilbert 1977; Hubel and Wiesel 1965; Kato et al. 1978; Rose 1977) or sides (Born and Tootell 1991; De Valois et al. 1985; Foster et al. 1985; Maffei and Fiorentini 1976; von der Heydt et al. 1992) of the classical receptive field, generating width and length tuning (DeAngelis et al. 1994; Sceniak et al. 2001). Surround stimuli at the ends can even enhance the classical receptive field response when coaligned with the classical receptive field stimulus, which is known as collinear facilitation (Kapadia et al. 1995, 2000; Polat et al. 1998). End-inhibition, also referred to as end-stopping, can be a mechanism to disambiguate motion and disparity information when viewed through the aperture created by receptive fields (Barth 2000; Heitger et al. 1992; Howe and Livingstone 2006; Lorenceau et al. 1993; Pack et al. 2003; Rubin et al. 1995; Yazdanbakhsh and Livingstone 2006), whereas collinear facilitation can be used to segment contours of an object across multiple receptive fields from complex backgrounds (Field et al. 1993; Kapadia et al. 1995; Li et al. 2006; Polat and Sagi 1993; Polat et al. 1998).

We wanted to test whether similar complex surround receptive field properties exist for neurons in the primary visual cortex (V1) of mice. If such behaviors were observed, the advanced genetic techniques that are available for mice could be leveraged to gain insight into the details and development of the circuits that underlie these response properties. We used two-photon imaging to measure the GCaMP6f calcium responses of V1 neurons while varying surround stimuli. We tested for differences in the response when the surround stimuli were displayed parallel to (lateral) or aligned with (collinear) the preferred orientation of the classical receptive field. Last, we examined the relationship between these complex surround properties and orientation tuning of individual neurons.

MATERIALS AND METHODS

Animal preparation and surgery. All procedures were approved by the Institutional Animal Care and Use Committee of Carnegie Mellon University and are in accordance with the National Institutes of Health

Address for reprint requests and other correspondence: J. M. Samonds, Center for Learning and Memory, University of Texas at Austin, Austin, TX 78712 (e-mail: samondjm@gmail.com).

Guide for the Care and Use of Laboratory Animals. We used 3% isoflurane to induce anesthesia in the mice and 1–2% isoflurane to maintain anesthesia during surgery. A heating pad was used to maintain a body temperature of 36.5°C, and the eyes were protected with mineral oil. To immobilize the head during imaging, a stainless steel bar was glued to the right side of the skull and secured with dental cement. A ~2.5-mm-diameter craniotomy was made over the visual cortex in the left hemisphere, identified by coordinates and landmarks as described in Kuhlman et al. (2011). We recorded data during six imaging sessions from four adult mice (2–4 mo old) expressing Cre recombinase (Cre) and red fluorescent protein (tdTomato) in parvalbumin (PV)-positive neurons, derived from a cross between PV-Cre knockin female mice (no. 008069; Jackson Laboratory; generated by S. Arber, Friedrich Miescher Institute) and male tdTomato reporter knockin mice (no. 007908, Ai14; Jackson Laboratory; generated by H. Zeng, Allen Institute for Brain Science). We used a glass micropipette attached to a Picospritzer III (Parker) to make a single tract injection with a total volume of 250–500 nl of the virus AAv9.Syn.GCaMP6f.WPRE.SV40 (no. AV-9-PV2822; Penn Vector Core, University of Pennsylvania) in the primary visual cortex. We injected 25–50 nl of virus every 50 μm, from 600 to 100 μm below the dural surface. The injection sites were later confirmed by intrinsic signal optical imaging as described below. We covered the craniotomy with a double glass assembly, where the diameter of the inner glass was fitted to the craniotomy, and sealed with dental cement. During recovery, mice were given 30 μl of 0.5 mg/ml carprofen via a subcutaneous injection.

Intrinsic signal optical imaging. At 7–14 days following craniotomy and injection, mice were anesthetized with 0.5% isofluorane and sedated with chlorprothixene (2 mg/kg). The craniotomy window was illuminated with a 630-nm LED (Prizmatix) and imaged with a tandem lens macroscope as in Pafundo et al. (2016). We acquired images at 30 frames per second using a 12-bit charge-coupled device camera (Dalsa 1M30), a frame grabber (Matrox Meteor II/Dig), and custom software. Frames were binned four times temporally and 2 × 2 spatially. We used two visual stimuli presented on an LCD monitor (40.5-cm width, 30-cm height) positioned 25 cm from the right eye at 70° to the long axis of the animal, covering −22° to 38° in elevation and −27° to 35° in azimuthal space. The stimuli presented were a horizontal white bar of 3° in height and a vertical white bar of 4° in width, drifting up or down and left or right, respectively, on a black background at 0.135 Hz. The drift speed was 10°/s, and the bar immediately returned to the screen after leaving it. We measured the vertical and horizontal retinotopy of V1 from phase maps calculated from the series of images generated by the drifting horizontal and vertical bar, respectively (Kalatsky and Stryker 2003). An image of the vasculature at the surface of the cortex was used to confirm that virus injections and two-photon microscopy were within V1. Receptive fields of calcium-imaged cells were within in the upper right visual field ranging from +20° to 60° horizontally and +5° to 20° vertically.

Data acquisition and calculation of response magnitude. In vivo imaging was performed on a two-photon microscope (Scientifica, Uckfield, UK), using a Chameleon Ultra II laser (Coherent) running at 930 nm and controlled by ScanImage 3 software (Vidrio Technologies; Pologruto et al. 2003). Image sequences (256 × 256 pixels, covering a field of view of 130 × 130 μm) were acquired at 2.05 Hz at a depth of 110–300 μm below the pia surface. During GCaMP6f imaging, red and green emissions were separated (dichroic FF568 and filter 510/84; Semrock) and detected simultaneously (Fig. 1*A*). PV interneurons were identified by their emission in the red channel and excluded from analysis (in all cases, the identified PV neurons failed the "no response" to surround-only test described below). During imaging, mice were anesthetized with 0.5% isoflurane and sedated with chlorprothixene (2 mg/kg).

Calcium signals of individual neurons were segmented using a deformable snake algorithm in which the fluorescent cytoplasmic ring was detected in a semiautomated manner (Kuhlman et al. 2013). Neurons were represented by the mean of 75–86 pixels, the nucleus was excluded, and no neuropil subtraction was performed. Response magnitude of individual neurons was calculated as $\Delta F/F_0$ = (peak response − baseline)/F_0. The peak response was defined as the peak value (1 frame) occurring during the stimulus presentation. Baseline was defined as the mean fluorescence across trials, 1 s preceding the stimulus onset (2 frames). One second of gray screen immediately following the stimulus termination was not included in the baseline calculation, thus minimizing contribution of still-decaying fluorescent signals. In addition to still-decaying signals, there are other factors that could increase baseline variability, including off responses and/or spontaneous activity. Given this potential for variability in baseline, some cells may not have been scored as significantly responding and excluded from the final data set. As such, our data set may be biased to those neurons that have short decay, no off response, and low spontaneous activity.

Visual stimuli. Stimuli were generated in MATLAB and displayed on a 20-in. LCD with a refresh rate of 60 Hz using Windows Media Player on full-screen mode (1,280 × 1,024 pixels) at a distance of 25 cm with a mean gray background of 30 cd/m^2. The timing of each

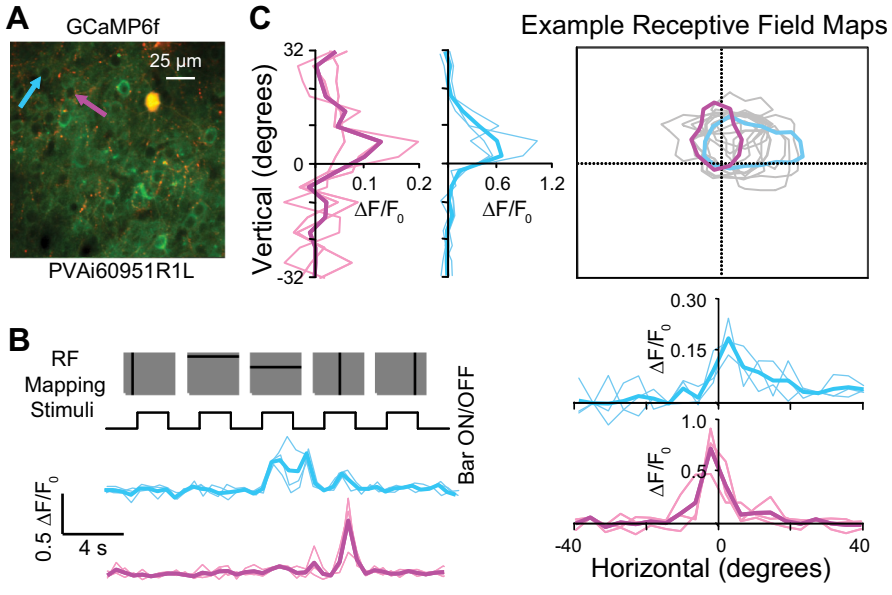

Fig. 1. Receptive field mapping. *A*: 2-photon GCaMP6f imaging within V1. PV-positive inhibitory neurons were labeled in red (yellow merge) and excluded from analysis. *B*: vertical and horizontal bars were used as stimuli to generate horizontal and vertical spatial tuning curves, respectively, for each neuron. Note that during surround modulation experiments, stimuli were randomly interleaved, and stimulus "off" responses were generally not observed and small when observed with smaller stimuli. *C*: examples of vertical and horizontal tuning curves based on the average of 3 trials (thin lines are single-trial responses). A contour of where the outer product of the tuning curves reaches less than 25% of its peak is shown to illustrate the 2-dimensional location of the receptive field with respect to the monitor. Twelve additional gray outlines of receptive fields are shown to illustrate the overlap within a single region from one session of two-photon imaging.

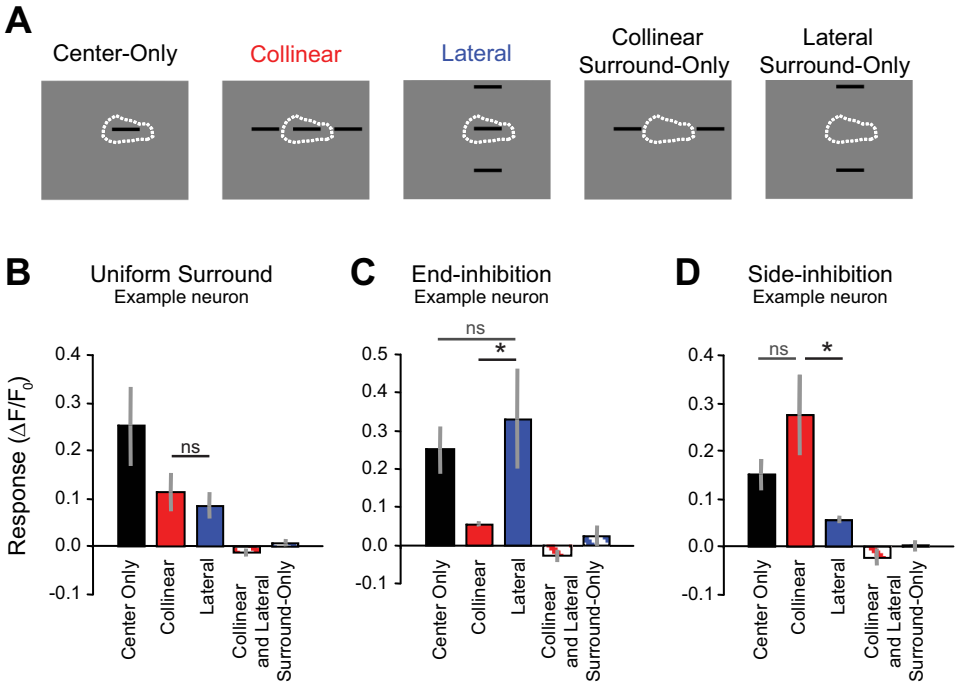

Fig. 2. Surround modulation of receptive field responses for 3 individual neurons. *A*: 5 conditions were used to test the spatial properties of surround modulation. *B–D*: example average peak responses across trial (error bars are SE) when stimuli were shown only within the receptive field (black) and when stimuli were shown both within the receptive field and the surround (red and blue) for uniform surround (*B*), end-inhibition (*C*), and side-inhibition (*D*). *$P < 0.05$ indicates the criteria used to score a neuron as nonuniform; "ns" indicates not significant, thereby signifying that nonuniform facilitation was not detected.

frame (e.g., stimulus onset and offset) was measured with a photodiode, and that data was synchronized to the two-photon data acquisition. To quickly determine the location and extent of classical receptive fields for individual neurons within the field of view before starting the surround modulation experiment in which 20 stimulus conditions were presented, we presented static black horizontal and vertical bars to the mice with lengths that covered the entire extent of the monitor for width and height, respectively, and had an approximate thickness of 4° of visual field. These bars were spaced at 4° and displayed for 2 s, and 2 s of mean gray screen were displayed between each black bar presentation (Fig. 1*B*). The mean response across four trials was measured for each neuron for each horizontal and vertical bar location to generate vertical and horizontal tuning curves, respectively (Fig. 1*C*). Our measured receptive field sizes are consistent with previous studies that found diameters ranged from 10° to 20° (Bonin et al. 2011; Niell and Stryker 2008; Roth et al. 2016).

To measure surround modulation, up to four stimuli locations were chosen during each imaging session that were aligned with the receptive fields of the most neurons that had local, robust, and reliable vertical and horizontal tuning curves (i.e., receptive field maps). An example of receptive field maps for 14 overlapping neurons acquired during one imaging session is shown in Fig. 1*C*. Once the receptive field location was determined, a single 15° × 2° bar at the center (Fig. 2*A*) was presented at four orientations (0°, 45°, 90°, and 135°). This was called the "center-only" condition. To test for end-inhibition, two bars (also 15° × 2°) were added outside of the classical receptive field location, each with their centers at a distance of 22.5° and coaligned to the bar in the center. This was called the "collinear" condition (Fig. 2*A*). Because these bars are 15° in length, the portions of the bars closest to the classical receptive field were always outside of a 30° diameter region centered on the classical receptive field. To test for side-inhibition, two bars were added outside of the classical receptive field location, each with their centers at a distance of 22.5° and parallel to the bar in the center. This was called the "lateral" condition (Fig. 2*A*). Finally, we tested the collinear and lateral surround conditions when there was no bar in the center ("surround-only" conditions) to make sure that the surround stimuli did not elicit a response and were indeed outside of the classical receptive field. Therefore, there were 5 conditions × 4 orientations for a total of 20 conditions for our experiment. The conditions were randomly interleaved for each trial. These stimuli were static and presented for 2 s with 2 s of mean gray screen between conditions. The distribution of nonuniform, side-inhibited, and end-inhibited neurons across animals is described in Table 1.

Data analysis. First, we identified responsive neurons using the following selection criteria: a given neuron was statistically responsive to the center-only condition (paired *t*-test, $P \leq 0.05$, $n = 5–40$ stimulus trials) and not responsive to either of the two surround-only conditions (paired *t*-test, $P > 0.05$, $n = 5–40$ stimulus trials). For this statistical testing, response was calculated as $\Delta F/F_0$ = (mean response − baseline)/F_0. In this case, mean response was used to avoid introducing statistical artifacts caused by selecting the maximum value during the response epoch and comparing with baseline. Baseline was defined as the mean fluorescence across trials, 1 s preceding the stimulus onset (2 frames). The mean response was defined as the mean value of the four frames occurring during the entire stimulus presentation. Each of the 20 stimulus conditions was presented for a minimum of 8 trials, typically 12–16 trials, and response magnitude was calculated. In one session, 40 trials were presented to confirm that asymmetric responses were maintained when a high number of trials was used. Given that we used light anesthesia, we noted that occasionally the animal blinked and that this seemed to correspond with an absence of response across the population. This observation was not verified by eye tracking. We examined the population response (mean of all neurons, across each frame that occurred during the stimulus presentation) to each of the trials. Trials in which there was no population

Table 1. *Distribution of neuron response types*

	Sample Size	Side-Inhibited	End-Inhibited	%Side	%End
Neuron count across mice	138	10	14	7	10
Neuron count by animal					
Mouse 1	13	3	2	23	15
Mouse 2	20	3	0	15	0
Mouse 3	3	0	1	0	33
Mouse 4	102	4	11	4	11

The distribution of nonuniform, side-inhibited, and end-inhibited neurons is described across animals.

average response were discarded; accounting for discarded trials, a minimum of five trials were analyzed per neuron. Trials with no population response were defined as those trials in which the mean F/F_0 value across all neurons within the field of view (where F is the instantaneous signal for a given frame and F_0 is defined as above) was less than zero, where trial refers to a single stimulus presentation. Only 21.9% of trials were discarded by this method. To assess whether the conclusions of this study could be impacted by the removal of these trials, the data were reanalyzed with all trials, and the results were similar: $n = 132$ significantly responding neurons (center only, $P < 0.05$); 30 of these 132 neurons had significant nonuniform surround, compared with 24 of 138 significantly responding neurons as reported using the no-population response discard method.

The four center-only conditions with orientations of 0°, 45°, 90°, and 135° were used to determine the preferred orientation and orientation selectivity of each neuron included in the surround modulation analysis. The preferred orientation was computed as the angle of the vector sum of the four responses R to each orientation θ:

$$\sum_k R_k e^{i2\theta_k} \quad (1)$$

The orientation selectivity index (OSI) was quantified as 1 – circular variance (CV) (Ringach et al. 2002):

$$\mathrm{OSI} = \frac{\left| \sum_k R_k e^{i2\theta_k} \right|}{\sum_k R_k} \quad (2)$$

For population averaging of orientation tuning curves, the data were aligned to the preferred orientation for each neuron. To compare orientation selectivity with surround properties, we computed a nonuniformity index (NUI), which was the difference between the responses to the collinear and lateral conditions at the preferred orientation divided by their sum. It is well documented that high levels of anesthesia reduce, and in many cases essentially eliminate, surround suppression. For example, a size-tuning study that examined surrounds encompassing a visual space up to 100° under heavy anesthesia found that the median population suppression index value was 0.04 (Self et al. 2014). The same study reported that the median population suppression index value increased to 0.37 under light urethane anesthesia, and some neurons reached suppression index values as high 0.65 under light anesthesia. Our population suppression index values are slightly lower yet similar to those reported in Self et al. (2014), and we also found individual neurons with suppression index values as high as 0.65. The maximum suppression index values that we observed were 0.77 and 0.76 for lateral and collinear surround, respectively. Considering that the surround stimulation used in this study encompassed 47°, which is smaller than in Self et al. (2014), most likely our animals are in a lightly anesthetized state.

RESULTS

Surround modulation is nonuniform for a subset of V1 neurons. To determine the proportion of neurons exhibiting either end- or side-stopping, we presented five stimulus conditions at four different orientations. Stimulus conditions consisted of center only, center + lateral parallel surround (lateral), center + collinear aligned surround (collinear), lateral surround only, and collinear surround only (Fig. 2*A*). We identified 138 neurons in 4 mice that were determined to be responsive to center-only stimuli (paired t-test $P < 0.05$). Mice were sedated with chlorprothixene and lightly anesthetized with isofluorane during visual stimulation. For most neurons, when we displayed flanking bars outside of the classical receptive field simultaneously with the center bar stimulus, the response was reduced compared with center bar-only stimulation. To quantify suppression, we computed a suppression index, similarly to Self et al. (2014). Under our conditions, the median suppression index across all neurons for the lateral condition was 0.29, and that for the collinear condition was 0.22. Generally, there was no significant difference between the suppression if we added bars coaligned (collinear) or parallel (lateral) to the bar within the classical receptive field (114 of 138 neurons, unpaired *t*-test, $P > 0.05$, $n = 5$–40 trials). An example of one of these neurons is shown on the left side of Fig. 2*B* and is described as receiving uniform suppression from the surround. The addition of collinear bars (red) or lateral bars (blue) resulted in suppression compared with when only a single bar was presented to the neuron (black). This surround suppression occurred even though there was no response to the collinear or lateral surround stimuli alone (red and white and blue and white).

Although most neurons responded like the example in Fig. 2*B*, there were clearly a noticeable number of neurons that responded very differently depending on whether the surrounding bars were presented collinearly or laterally. For the example neuron in Fig. 2*C*, the classical receptive field response (black) was strongly suppressed (unpaired *t*-test, $P = 0.02$, $n =$ 6 and 7 trials) when collinear bars were added to the surround (red), but there was no suppression and maybe even an enhancement of the response (although not significant, unpaired *t*-test, $P = 0.57$, $n = 5$ and 7 trials) when lateral bars were added to the surround (blue). In this case, there was "end-inhibition" from the surround. For the example neuron in Fig. 2*D*, the classical receptive field response (black) was strongly suppressed (unpaired *t*-test, $P = 0.02$, $n = 6$ and 7 trials) when lateral bars were added to the surround (blue), but there was no suppression and maybe even an enhancement of the response (although not significant, unpaired *t*-test, $P = 0.16$, $n = 5$ and 7 trials) when collinear bars were added to the surround (red). In this case, there was "side-inhibition" from the surround. Again, there was no significant response to the collinear or lateral surrounds alone (red and white or blue and white, respectively) for either of these two nonuniform surround example neurons (Fig. 2*C*, $P = 0.18$ and 0.52; Fig. 2*D*, $P =$ 0.27 and 0.99).

We characterized the nonuniformity of surround modulation for each of 138 neurons that had a significant classical receptive field response and no significant response to either of the surround-only conditions (see MATERIALS AND METHODS). The comparisons of the mean peak responses to the collinear (vertical axis) and lateral (horizontal axis) conditions are shown in Fig. 3. For 24 neurons (17%), there was a significantly different response to these two conditions (unpaired *t*-test, $P \leq 0.05$, $n = 5$–40 trials). The blue data points ($n = 14$ neurons) are represented by the example in Fig. 2*C* demonstrating end-inhibition, and the red data points ($n = 10$ neurons) are represented by the example in Fig. 2*D* demonstrating side-inhibition. Data points along the principal diagonal are represented by the example in Fig. 2*B* demonstrating uniform suppression.

Surround modulation is predominately suppressive. In Fig. 2, *B–D*, we labeled our examples in terms of the type of surround suppression they exhibited, but some responses shown in the examples also suggest the possibility that our stimuli caused surround facilitation. Because Fig. 3 only shows

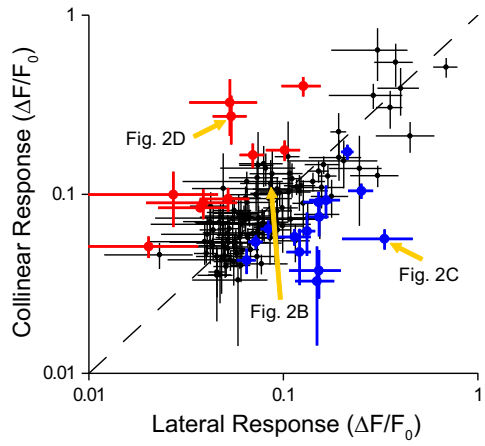

Fig. 3. Nonuniformity of surround modulation. For some neurons, the response to stimulus within the classical receptive field was significantly greater ($P < 0.05$) with bars in the collinear (lateral) surround regions vs. the lateral (collinear) surround regions (red and blue data points, respectively). Error bars are SE with respect to trials. Examples from Fig. 2 are noted by gold arrows.

the comparison of the responses between the collinear and lateral stimuli conditions without respect to the center-only condition, we also directly compared the surround to the center-only condition. The data for all neurons are shown in Fig. 4, *A* and *B*. The pink data points compare responses between the collinear (vertical axis) and center-only (horizontal axis) stimuli, whereas the light blue data points compare responses between the lateral and center-only stimuli. Most data points fell below the principal diagonal, confirming that the surround primarily suppresses the classical receptive field response. In the collinear surround condition, the classical receptive field response was significantly suppressed in 41 neurons and significantly facilitated in only 1 neuron; in the lateral surround condition, the classical receptive field response was significantly suppressed in 30 neurons (unpaired *t*-test, $P \leq 0.05$, $n = 5$–40 trials).

For the 14 neurons represented by the blue data points in Fig. 3, we highlighted their data points in Fig. 4*A* by making them red and dark blue to show whether they were suppressed or facilitated by collinear and lateral surrounds, respectively. The results demonstrate that these neurons had little or no suppression for the lateral surround (dark blue data points) and were strongly suppressed by the collinear surround (red data points). For the 10 neurons represented by the red data points in Fig. 3, we highlighted their data points in Fig. 4*B* by making them red and dark blue to show whether they were suppressed or facilitated by collinear and lateral surrounds, respectively. The results clearly show that these neurons had little or no suppression for the collinear surround (red data points) and were strongly suppressed by the lateral surround (dark blue data points).

Neurons with nonuniform surround modulation have greater orientation selectivity. Properties such as the total stimulus size and the orientation of contours in the surround region outside of the classical receptive field can influence orientation selectivity (Chen et al. 2005; Knierim and van Essen 1992; Nelson and Frost 1978; Self et al. 2014; Xing et al. 2005), so we examined whether there was a relationship between nonuniform surround properties and orientation selectivity. Figure 5*A* illustrates that our sample of 138 neurons provided us with neurons tuned for all possible orientations with a bias for horizontal orientations that has been previously reported in mice (Dräger 1975; Scholl et al. 2013; Yoshida et al. 2012). We measured the orientation selectivity index (OSI; see MATERIALS AND METHODS) for all 138 neurons. If a neuron responded to only a single orientation, the OSI is equal to 1. If a neuron responded to every orientation equally, the OSI is 0. OSI was then compared with a nonuniformity index (NUI). NUI quantifies the nonuniformity of the surround as the difference between the responses to the collinear and lateral conditions at the preferred orientation of each neuron divided by their sum. A negative NUI means that the neuron preferred a lateral surround and was suppressed more by a collinear surround, i.e., end-inhibited, whereas a positive NUI means that the neuron preferred a collinear surround and was suppressed more by a lateral surround, i.e., side-inhibited. We did not detect a relationship between type of asymmetry and preferred orientation (Fig. 5*B*). However, we did detect a relationship between NUI and orientation selectivity (Fig. 5*C*).

The scatter plot in Fig. 5*C* shows that OSI and nonuniformity of the surround were correlated. NUI and OSI were significantly negatively correlated for negative NUI values (blue data points; $r = -0.32$, 1-sample *t*-test, $P = 0.004$, $n = 78$ neurons) and significantly positively correlated for positive NUI values (red data points; $r = 0.31$, 1-sample *t*-test, $P = 0.02$, $n = 60$ neurons). We divided the data into three groups of neurons on the basis of NUI values and computed a population average (see MATERIALS AND METHODS) and found

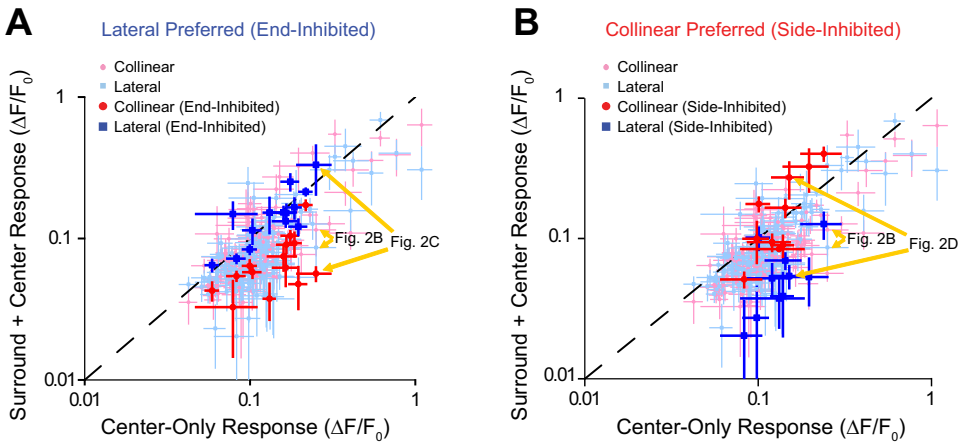

Fig. 4. Nonuniformity arises from lack of suppression in particular surround regions. *A*: neurons that respond significantly greater ($P < 0.05$) to classical receptive field stimuli with bars in the lateral surround are end-inhibited: they are strongly suppressed by collinear bars (red) with little or no suppression by lateral bars (blue). *B*: neurons that respond significantly greater ($P < 0.05$) to classical receptive field stimuli with bars in the collinear surround are side-inhibited: they are strongly suppressed by lateral bars (blue) with little or no suppression by collinear bars (red). Error bars are SE with respect to trials. Examples from Fig. 2 are noted by gold arrows.

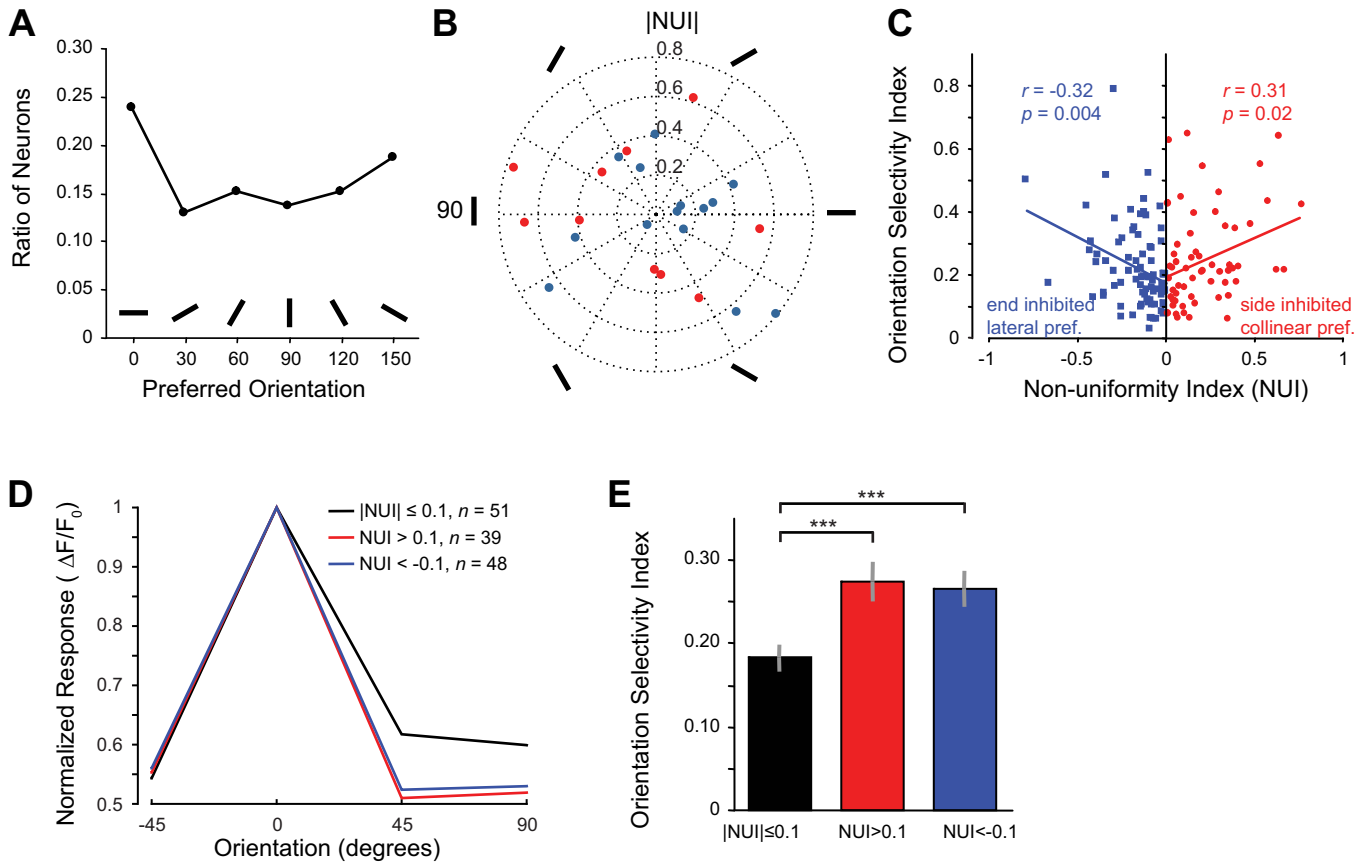

Fig. 5. Neurons with stronger nonuniformity in surround modulation have sharper orientation tuning. *A*: distribution of preferred orientations (there is a slight bias for horizontal orientations, 0°). Preferred orientation was calculated from the vector sum of the responses to the 4 orientations presented and binned into 6 groups. *B*: preferred orientations for all 24 significantly side- and end-inhibited neurons. Preferred orientation was calculated from the vector sum of the responses to the 4 orientations presented. NUI, nonuniformity index. *C*: orientation selectivity increases with greater nonuniformity in surround modulation for both lateral ($n = 79$, blue) and collinear ($n = 59$, red) condition-preferring neurons. *D*: population averages of orientation tuning divided into 3 groups on the basis of surround modulation nonuniformity. *E*: average orientation selectivity for the same 3 groups (error bars are SE based on neurons). ***$P < 0.001$.

that orientation tuning was more selective for neurons with negative or positive NUI values (Fig. 5*D*, blue and red curves) compared with neurons with uniform surrounds (Fig. 5*D*, black curve; NUI close to 0). This result is reflected by average OSI measurements for these same three groups of neurons (Fig. 5*E*). Nonuniform surround neurons (red and blue) had significantly higher OSI values (Kruskal-Wallis test, $P < 0.001$; Wilcoxon rank sum uncorrected for 2 multiple comparisons, collinear vs. uniform: $P = 0.001$ for $n = 39$ and 51 neurons, respectively; lateral vs. uniform: $P = 0.001$ for $n = 48$ and 51 neurons, respectively) than uniform surround neurons (black). We noted that the average response magnitude was larger in the nonuniform surround condition (collinear: 0.13 ± 0.02, lateral: 0.12 ± 0.01) at preferred orientations compared with uniform surround neurons (0.11 ± 0.01); this difference was not significant (Kruskal-Wallis test, $P = 0.52$; Wilcoxon rank sum uncorrected for multiple comparisons, collinear vs. uniform: $P = 0.16$ for $n = 39$ and 51 neurons, respectively; lateral vs. uniform: $P = 0.96$ for $n = 48$ and 51 neurons, respectively). However, given that saturating nonlinearities of calcium responses, in relation to the actual spike response (Chen et al. 2013; Nauhaus et al. 2012), have the potential to artificially create a correlation between orientation selectivity and response magnitude, we wanted to make sure that the significantly larger OSI values found in nonuniform surround neurons were not an artifact of larger responses. First, we directly examined the relationship between OSI and the mean response to the preferred orientation for our data. There was no significant correlation between these measurements (Fig. 6*A*; $r = 0.13$, 1-sample *t*-test, $P = 0.14$, $n = 138$ neurons). In addition, we removed data points with the largest values until the average response for nonuniform surround neurons were equal to or less than the responses for uniform surround neurons. This required us only to remove one neuron from the collinear surround data and three neurons from the lateral surround data. The orientation selectivity was still sharper for the neurons with high positive or negative NUI values (Fig. 6*C*, red and blue) compared with neurons with low NUI values (Fig. 6*C*, black). We still observed significantly larger OSI values for nonuniform surround neurons (red and blue) compared with uniform surround neurons (black) even though the responses for nonuniform surround neurons were less than or equal to the responses of the uniform surround neurons (Fig. 6*C*; Kruskal-Wallis test, $P < 0.001$; Wilcoxon rank sum, collinear vs. uniform: $P = 0.001$ for $n = 38$ and 51 neurons, respectively; lateral vs. uniform: $P = 0.0025$ for $n = 45$ and 51 neurons, respectively).

Increases in trial-to-trial noise combined with a limited number of observations could also increase the chances of observing higher OSI or NUI values, which could lead to a

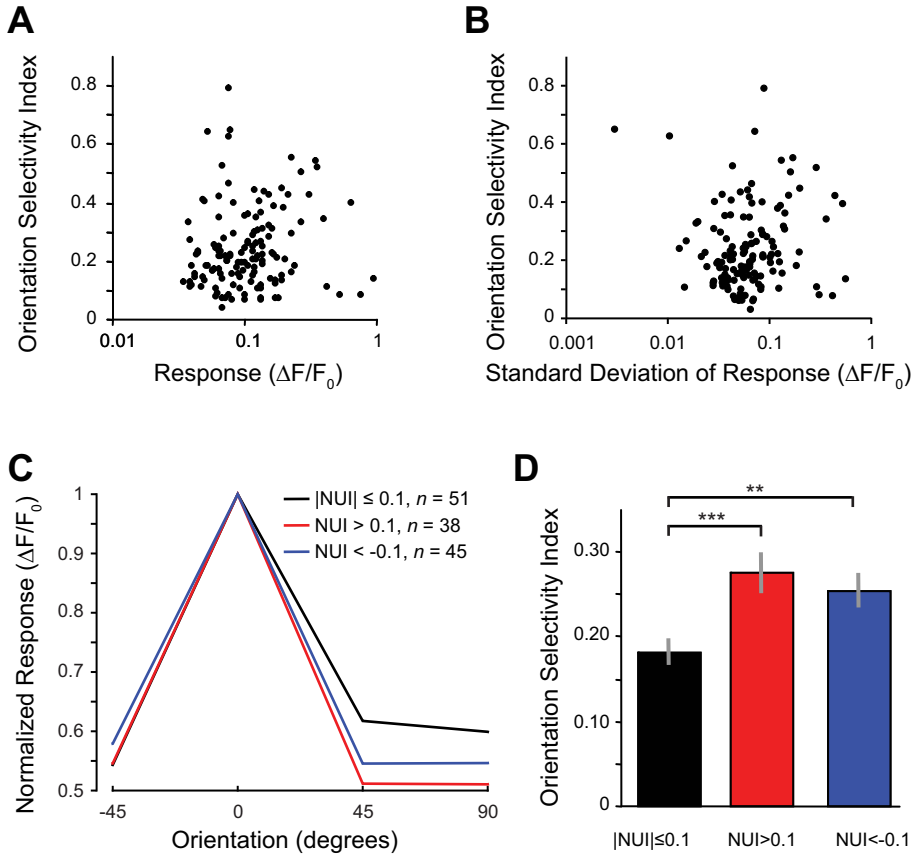

Fig. 6. Orientation selectivity does not depend or response magnitude. *A*: there is no significant correlation between orientation selectivity and response magnitude. *B*: there is no significant correlation between orientation selectivity and response noise. *C*: high-response data points for nonuniform surround neurons were dropped so that the average response magnitude for nonuniform surround neurons was less than or equal to the average response of uniform surround neurons. *D*: average orientation selectivity for the same 3 groups remained similar to that observed in Fig. 5 (error bars are SE based on neurons). $^{**}P < 0.01$; $^{***}P < 0.001$.

correlation between the measurements. Therefore, we examined the relationship between OSI and the standard deviation of responses to the preferred orientation and found no significant correlation (Fig. 6*B*; $r = 0.05$, 1-sample *t*-test, $P = 0.56$, $n = 138$ neurons). There was also no significant correlation between negative NUI values and the standard deviation of response magnitude ($r = -0.19$, 1-sample *t*-test, $P = 0.17$, $n = 78$ neurons) or positive NUI values and the standard deviation of response magnitude ($r = 0.18$, 1-sample *t*-test, $P = 0.10$, $n = 60$ neurons).

Surround modulation nonuniformity is robust to changes in surround configuration. The variability in receptive field size and shape, as well as the scatter in receptive field location (e.g., Fig. 1*C*), can make it difficult to precisely characterize surround modulation for a large population of neurons simultaneously. We attempted to carefully choose stimuli center locations that were optimal for the largest number of receptive fields. Sometimes the collinear and lateral surround conditions were, nonetheless, at different distances from the classical receptive field (e.g., Fig. 2*A*). For 93 neurons, we included an additional lateral surround condition, "lateral close," where the two surround bars were moved 7.5° closer to the center compared with the original lateral condition, "lateral far" (Fig. 7*A*). There was not a significant difference between the responses to the lateral close and lateral far conditions (Wilcoxon signed rank, $P = 0.19$, $n = 93$ neurons), and the responses were highly correlated between the two conditions (Fig. 7*A*; $r = 0.85$, $P < 0.001$). Similarly, there was not a significant difference in NUI values between the lateral close and lateral far conditions (Wilcoxon signed rank, $P = 0.70$, $n = 93$ neurons), and NUI values between the two conditions were significantly correlated (Fig. 7*B*; $r = 0.36$, $P < 0.001$). With the use of both the lateral close and far conditions, there was no significant bias of nonuniform surround modulation toward the lateral or collinear surround conditions (Wilcoxon signed rank, $P = 0.83$ and 0.63, respectively, $n = 93$ neurons). The width of the distributions was also not different between the two conditions, suggesting that the amount of nonuniformity was unaffected by moving the bars closer to the receptive field (Fig. 7*C*). Finally, we examined if changing the position of the surround stimuli had a significant impact on the relationship between nonuniformity of the surround and orientation selectivity. Figure 7*D* shows the same results as Fig. 5*C* when this smaller set of data is used. Again, there is a significant negative correlation between orientation selectivity and NUI values for neurons with negative NUI values (blue data points; $r = -0.41$, $P = 0.003$, $n = 51$ neurons) and significant positive correlation for neurons with positive NUI values (red data points; $r = 0.32$, $P = 0.04$, $n = 42$ neurons). When the lateral bars were moved closer to the receptive field, the correlation was still negative for neurons with negative NUI values (light blue data points; $r = -0.24$, $P = 0.09$, $n = 49$ neurons) and positive for neurons with positive NUI values (pink data points; $r = 0.36$, $P = 0.02$, $n = 44$ neurons). Overall, the distribution of nonuniform surround modulation and the relationship between nonuniform surround modulation and orientation selectivity were fairly robust to changes in the precise position of the surround elements.

DISCUSSION

Similar to what has been observed in higher species, such as primates and carnivores, we found that neurons in the primary

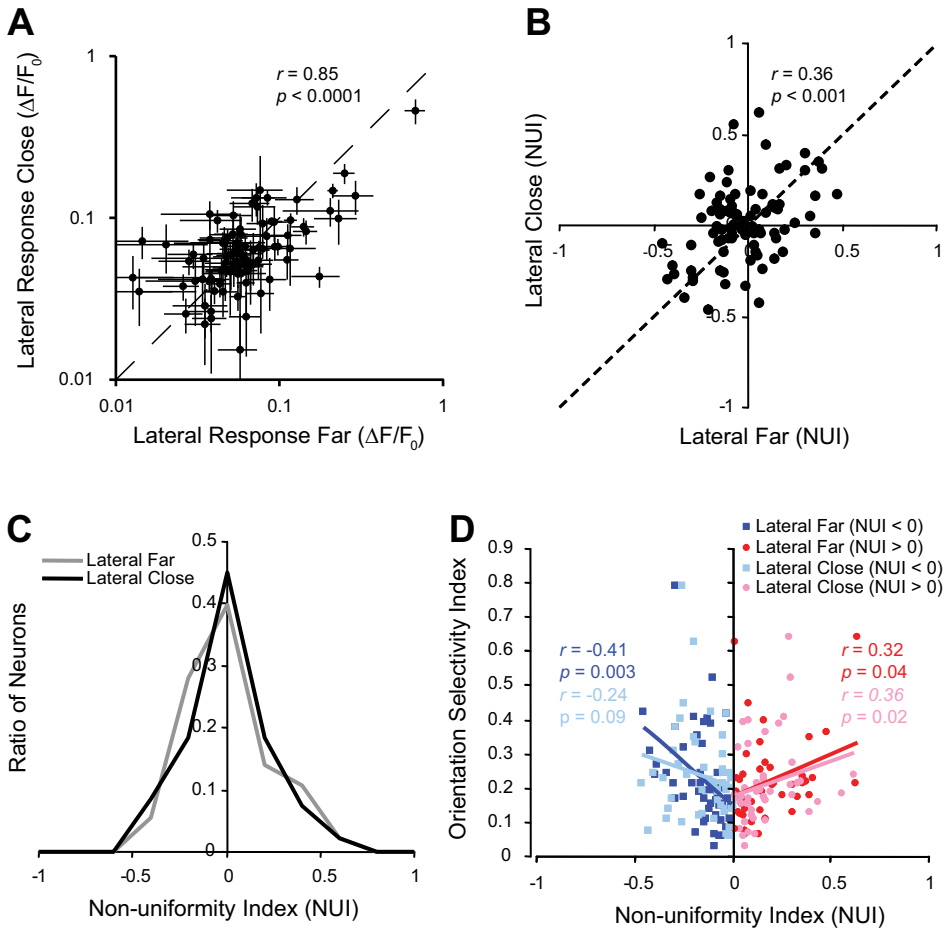

Fig. 7. Surround modulation nonuniformity is robust to changes in surround configuration. *A*: comparison of response magnitudes when the lateral surround is closer to (lateral close) or farther from (lateral far) the receptive field (*inset*). *B*: comparison of the nonuniformity index (NUI) between the lateral close and lateral far conditions. *C*: comparison of the distributions of NUIs for the lateral close and lateral far conditions. *D*: comparison of correlation between orientation selectivity and NUI between the lateral close and lateral far conditions.

visual cortex of mice exhibit complex surround modulation. Although stimulation beyond the classical receptive field generally caused suppression regardless of the location (uniform surround suppression), there were clearly some neurons that were suppressed in only certain regions of the surround (nonuniform surround suppression). Based on our set of stimuli, these particular regions were either the collinear surrounds (end-inhibition) or the lateral surrounds (side-inhibition). Last, we also found that those neurons that were either end-inhibited or side-inhibited generally had more selective orientation tuning. This raises the possibility that these two properties of V1 neurons might be linked in some way either functionally or through their development.

Comparison to previous studies in other species. Several classical studies have observed end-inhibition (Dreher 1972; Gilbert 1977; Hubel and Wiesel 1965; Kato et al. 1978; Rose 1977) or side-inhibition (Born and Tootell 1991; De Valois et al. 1985; Foster et al. 1985; Maffei and Fiorentini 1976; von der Heydt et al. 1992) in V1 of cats and monkeys. The most comprehensive study of both end and side-inhibition was based on recordings in cat V1 (DeAngelis et al. 1994), which reported results that are very consistent with what we observed in our two-photon imaging data from mouse V1. DeAngelis et al. (1994) also found that the surround was generally suppressive and that the suppression was generally uniform, although there were subclasses of neurons that only exhibited surround suppression at the ends and sides of the classical receptive field. We found a lower percentage of end- and side-inhibited neurons compared with what was reported in the cat, and the surround suppression that we observed was weaker. We used a more limited set of stimuli that were not optimized for each neuron compared with those used by DeAngelis et al. (1994). If our receptive field stimuli did not drive some neurons sufficiently or our surround stimuli did not drive surrounding neurons sufficiently because they were not optimal, we might have underestimated the suppression and missed some neurons with end- and side-inhibition. For example, we chose a very conservative definition of the surround for all neurons to make sure that surround stimuli did not encroach on the classical receptive field for individual neurons. In addition, there may be genuine differences between the cat and mouse with respect to end- and side-inhibition because cats have greater orientation selectivity than mice (Scholl et al. 2013; Tan et al. 2011), and our results in Fig. 5*C* suggest a link between greater surround nonuniformity and greater orientation selectivity.

Although the results from DeAngelis et al. (1994) and our present results showed that the surround was almost always suppressive, several studies have found that the surround can be facilitative, as well (Jones et al. 2001; Kapadia et al. 1995; Levitt and Lund 1997; Polat et al. 1998; Sceniak et al. 1999). First, for some neurons in primate and mouse V1, if an orientation orthogonal to the preferred orientation is presented in the surround with the preferred orientation presented in the classical receptive field, responses are stronger than if only the preferred orientation is displayed in the classical receptive field (Hupé et al. 2001; Jones et al. 2001; Self et al. 2014). Second,

the surround at far distances from the classical receptive field in primate V1 neurons can be facilitative (Ichida et al. 2007; Schwabe et al. 2010; Shushruth et al. 2009). Third, if the contrast of the stimulus is reduced, the surround can change from being suppressive to facilitative (Levitt and Lund 1997; Sceniak et al. 1999). Last, neurons in cats and primates with side-inhibition can exhibit end or collinear facilitation (Kapadia et al. 1995; Polat et al. 1998). We did find one neuron with significant collinear facilitation, and DeAngelis et al. (1994) did note that some side-inhibited neurons had very long receptive fields.

There could be multiple reasons why we did not observe significant facilitation for more of these neurons. First, we only used surround conditions where the orientation of the surround elements matched the orientation of the center bar and did not test receptive field responses with a contrasting surround (Hupé et al. 2001; Jones et al. 2001; Self et al. 2014). Second, collinear facilitation is clearer when the contrast of the center bar is reduced (Polat et al. 1998), and we used only high-contrast bars. Third, collinear facilitation is delayed compared with the classical receptive field response and surround suppression (Li et al. 2006); given the slower temporal dynamics of calcium imagining, it is possible the presence of facilitation was not detected. Finally, DeAngelis et al. (1994) noted that the neurons with long receptive fields and prominent side-inhibition were predominantly located in layer 6 (see also Bolz and Gilbert 1986; Gilbert 1977), whereas our imaging was restricted to cortical layer 2/3.

Previous studies in other species have not explicitly described a relationship between end- or side-inhibition and orientation selectivity. The one exception that is consistent with our results is a report by Henry et al. (1974), who found that hypercomplex cells (end-inhibited) have a narrower bandwidth compared with simple and complex cells, based on a small sample of five hypercomplex cells. However, there are several studies in cats and primates that do implicate surround modulation of orientation tuning as playing an important role in orientation-based perception. First, increasing stimulus size (and presumably surround modulation), as well as stimulation of the nonclassical receptive field, sharpens orientation tuning (Chen et al. 2005; Xing et al. 2005). Second, end-inhibition has been suggested as a possible mechanism to disambiguate the direction of motion within the classical receptive field (Pack et al. 2003). Finally, collinear facilitation and side-inhibition have been proposed to help detect and group orientated contours within complex backgrounds (Kapadia et al. 1995; Li et al. 2006; Polat et al. 1998). All of these results indicate that there should be a relationship between complex surround properties and orientation tuning, which we demonstrated in Fig. 5.

Potential underlying circuitry. Even those neurons with uniform surround suppression have highly complex surround properties. Several studies in the primate and cat have found that there are multiple concentric surround regions with modulations of the classical receptive field response that are tuned and untuned for spatiotemporal properties such as orientation, spatial frequency, and temporal frequency (Angelucci et al. 2002; Angelucci and Bullier 2003; Hashemi-Nezhad and Lyon 2012; Nurminen and Angelucci 2014; Webb et al. 2005). The sources of these surround modulations include feedforward, feedback, and horizontal synaptic inputs and serve different functional purposes.

The addition of the nonuniform properties described in this article adds an additional dimension to this already complex surround. Numerous experiments and models have led to a wide range of potential circuits that could generate or contribute to end-inhibition that include only feedforward excitatory inputs (Skottun 1998; Skottun 2005), feedback inhibition from neurons with larger receptive fields (Anderson et al. 2001; Bolz and Gilbert 1986), or feedback facilitation from neurons with smaller receptive fields (Grieve and Sillito 1991). These studies address the source of the suppression at the ends or length tuning and do not answer the question of why there is a lack of suppression on the sides. Presumably, for side-inhibited neurons, similar circuitry could explain their suppression, and the lack of suppression on the ends could be explained by collinear facilitation (Kapadia et al. 1995; Polat et al. 1998) from horizontal inputs (Crook et al. 2002). We propose that two distinct mechanisms could be responsible for the asymmetry observed in the present study. First, both end- and side-inhibited neurons would have uniform surround suppression that could be generated by the inhibitory interneurons described by Adesnik et al. (2012) and Nienborg et al. (2013). Second, lateral and collinear facilitation would produce the nonuniformity for end- and side-inhibited neurons, respectively.

Conclusions. We describe nonuniform suppressive surrounds with end and side suppression that have been previously reported in cats and primates. These properties have important perceptual implications as mechanisms to disambiguate motion and disparity (Barth 2000; Heitger et al. 1992; Howe and Livingstone 2006; Lorenceau et al. 1993; Pack et al. 2003; Rubin et al. 1995; Yazdanbakhsh and Livingstone 2006), as well as detecting and segmenting object contours (Field et al. 1993; Kapadia et al. 1995; Li et al. 2006; Polat and Sagi 1993; Polat et al. 1998), and the surround properties and mechanisms are consistent with a more general model of predictive coding (Rao and Ballard 1999; Seriès et al. 2003; Spratling 2010). The significance of finding these properties in the mouse visual cortex is that the mouse preparation currently offers an unprecedented ability to decipher the detailed circuitry on the basis of cell types and very specific connectivity (e.g., Jia et al. 2010; Ko et al. 2011, 2013; Zhang et al. 2014) that underlies perceptual functions such as gain control (Atallah et al. 2012; Scholl et al. 2015; Wilson et al. 2012). The short life cycle of the mouse also offers advantages in studying the development of these circuits, and because end- and side-inhibition are related to orientation selectivity, there are likely interesting changes to their underlying circuitry during both the critical period (Kuhlman et al. 2011) and adulthood (Poort et al. 2015; Yoshida et al. 2012).

ACKNOWLEDGMENTS

We appreciate the technical assistance provided by Diego Pafundo and Yuke Li.

Present address of J. M. Samonds: Center for Learning and Memory, University of Texas at Austin, Austin, TX 78712.

GRANTS

This work was supported by National Institutes of Health (NIH) Grant R01EY022247 (to T. S. Lee), National Science Foundation Award 1320651 (to T. S. Lee), and NIH Grant 1R01EY024678 (to S. J. Kuhlman), and by

Intelligence Advanced Research Projects Activity (IARPA) via Department of Interior/Interior Business Center (DoI/IBCContract D16PC00007.

DISCLAIMERS

The views and conclusions contained herein are those of the authors and should not be interpreted as necessarily representing the official policies or endorsements, either expressed or implied, of IARPA, DoI/IBC, or the U.S. Government (TSL and SJK). The U.S. Government is authorized to reproduce and distribute reprints for Governmental purposes notwithstanding any copyright annotation thereon.

DISCLOSURES

No conflicts of interest, financial or otherwise, are declared by the authors.

AUTHOR CONTRIBUTIONS

J.M.S., T.S.L., and S.J.K. conceived and designed research; J.M.S. and B.D.F. performed experiments; J.M.S. and B.D.F. analyzed data; J.M.S., T.S.L., and S.J.K. interpreted results of experiments; J.M.S. and S.J.K. prepared figures; J.M.S. drafted manuscript; J.M.S., T.S.L., and S.J.K. edited and revised manuscript; J.M.S. and S.J.K. approved final version of manuscript.

REFERENCES

Adesnik H, Bruns W, Taniguchi H, Huang ZJ, Scanziani M. A neural circuit for spatial summation in visual cortex. *Nature* 490: 226–231, 2012. doi:10.1038/nature11526.

Allman J, Miezin F, McGuinness E. Stimulus specific responses from beyond the classical receptive field: neurophysiological mechanisms for local-global comparisons in visual neurons. *Annu Rev Neurosci* 8: 407–430, 1985. doi:10.1146/annurev.ne.08.030185.002203.

Anderson JS, Lampl I, Gillespie DC, Ferster D. Membrane potential and conductance changes underlying length tuning of cells in cat primary visual cortex. *J Neurosci* 21: 2104–2112, 2001.

Angelucci A, Bullier J. Reaching beyond the classical receptive field of V1 neurons: horizontal or feedback axons? *J Physiol Paris* 97: 141–154, 2003. doi:10.1016/j.jphysparis.2003.09.001.

Angelucci A, Levitt JB, Walton EJ, Hupe JM, Bullier J, Lund JS. Circuits for local and global signal integration in primary visual cortex. *J Neurosci* 22: 8633–8646, 2002.

Atallah BV, Bruns W, Carandini M, Scanziani M. Parvalbumin-expressing interneurons linearly transform cortical responses to visual stimuli. *Neuron* 73: 159–170, 2012. doi:10.1016/j.neuron.2011.12.013.

Barth E. A geometric view on early and middle level visual coding. *Spat Vis* 13: 193–199, 2000. doi:10.1163/156856800741207.

Bolz J, Gilbert CD. Generation of end-inhibition in the visual cortex via interlaminar connections. *Nature* 320: 362–365, 1986. doi:10.1038/320362a0.

Bonin V, Histed MH, Yurgenson S, Reid RC. Local diversity and fine-scale organization of receptive fields in mouse visual cortex. *J Neurosci* 31: 18506–18521, 2011. doi:10.1523/JNEUROSCI.2974-11.2011.

Born RT, Tootell RB. Single-unit and 2-deoxyglucose studies of side inhibition in macaque striate cortex. *Proc Natl Acad Sci USA* 88: 7071–7075, 1991. doi:10.1073/pnas.88.16.7071.

Cavanaugh JR, Bair W, Movshon JA. Nature and interaction of signals from the receptive field center and surround in macaque V1 neurons. *J Neurophysiol* 88: 2530–2546, 2002a. doi:10.1152/jn.00692.2001.

Cavanaugh JR, Bair W, Movshon JA. Selectivity and spatial distribution of signals from the receptive field surround in macaque V1 neurons. *J Neurophysiol* 88: 2547–2556, 2002b. doi:10.1152/jn.00693.2001.

Chen G, Dan Y, Li CY. Stimulation of non-classical receptive field enhances orientation selectivity in the cat. *J Physiol* 564: 233–243, 2005. doi:10.1113/jphysiol.2004.080051.

Chen TW, Wardill TJ, Sun Y, Pulver SR, Renninger SL, Baohan A, Schreiter ER, Kerr RA, Orger MB, Jayaraman V, Looger LL, Svoboda K, Kim DS. Ultrasensitive fluorescent proteins for imaging neuronal activity. *Nature* 499: 295–300, 2013. doi:10.1038/nature12354.

Crook JM, Engelmann R, Löwel S. GABA-inactivation attenuates colinear facilitation in cat primary visual cortex. *Exp Brain Res* 143: 295–302, 2002. doi:10.1007/s00221-002-1007-y.

De Valois RL, Thorell LG, Albrecht DG. Periodicity of striate-cortex-cell receptive fields. *J Opt Soc Am A* 2: 1115–1123, 1985. doi:10.1364/JOSAA.2.001115.

DeAngelis GC, Freeman RD, Ohzawa I. Length and width tuning of neurons in the cat's primary visual cortex. *J Neurophysiol* 71: 347–374, 1994.

Dräger UC. Receptive fields of single cells and topography in mouse visual cortex. *J Comp Neurol* 160: 269–289, 1975. doi:10.1002/cne.901600302.

Dreher B. Hypercomplex cells in the cat's striate cortex. *Invest Ophthalmol* 11: 355–356, 1972.

Field DJ, Hayes A, Hess RF. Contour integration by the human visual system: evidence for a local "association field". *Vision Res* 33: 173–193, 1993. doi:10.1016/0042-6989(93)90156-Q.

Foster KH, Gaska JP, Nagler M, Pollen DA. Spatial and temporal frequency selectivity of neurones in visual cortical areas V1 and V2 of the macaque monkey. *J Physiol* 365: 331–363, 1985. doi:10.1113/jphysiol.1985.sp015776.

Gilbert CD. Laminar differences in receptive field properties of cells in cat primary visual cortex. *J Physiol* 268: 391–421, 1977. doi:10.1113/jphysiol.1977.sp011863.

Grieve KL, Sillito AM. A re-appraisal of the role of layer VI of the visual cortex in the generation of cortical end inhibition. *Exp Brain Res* 87: 521–529, 1991. doi:10.1007/BF00227077.

Guo K, Robertson RG, Mahmoodi S, Young MP. Centre-surround interactions in response to natural scene stimulation in the primary visual cortex. *Eur J Neurosci* 21: 536–548, 2005. doi:10.1111/j.1460-9568.2005.03858.x.

Hashemi-Nezhad M, Lyon DC. Orientation tuning of the suppressive extraclassical surround depends on intrinsic organization of V1. *Cereb Cortex* 22: 308–326, 2012. doi:10.1093/cercor/bhr105.

Heitger F, Rosenthaler L, von der Heydt R, Peterhans E, Kübler O. Simulation of neural contour mechanisms: from simple to end-stopped cells. *Vision Res* 32: 963–981, 1992. doi:10.1016/0042-6989(92)90039-L.

Henry GH, Dreher B, Bishop PO. Orientation specificity of cells in cat striate cortex. *J Neurophysiol* 37: 1394–1409, 1974.

Howe PDL, Livingstone MS. V1 partially solves the stereo aperture problem. *Cereb Cortex* 16: 1332–1337, 2006. doi:10.1093/cercor/bhj077.

Hubel DH, Wiesel TN. Receptive fields and functional architecture in two nonstriate visual areas (18 and 19) of the cat. *J Neurophysiol* 28: 229–289, 1965.

Hupé J-M, James AC, Girard P, Bullier J. Response modulations by static texture surround in area V1 of the macaque monkey do not depend on feedback connections from V2. *J Neurophysiol* 85: 146–163, 2001.

Ichida JM, Schwabe L, Bressloff PC, Angelucci A. Response facilitation from the "suppressive" receptive field surround of macaque V1 neurons. *J Neurophysiol* 98: 2168–2181, 2007. doi:10.1152/jn.00298.2007.

Jia H, Rochefort NL, Chen X, Konnerth A. Dendritic organization of sensory input to cortical neurons in vivo. *Nature* 464: 1307–1312, 2010. doi:10.1038/nature08947.

Jones HE, Grieve KL, Wang W, Sillito AM. Surround suppression in primate V1. *J Neurophysiol* 86: 2011–2028, 2001.

Kalatsky VA, Stryker MP. New paradigm for optical imaging: temporally encoded maps of intrinsic signal. *Neuron* 38: 529–545, 2003. doi:10.1016/S0896-6273(03)00286-1.

Kapadia MK, Ito M, Gilbert CD, Westheimer G. Improvement in visual sensitivity by changes in local context: parallel studies in human observers and in V1 of alert monkeys. *Neuron* 15: 843–856, 1995. doi:10.1016/0896-6273(95)90175-2.

Kapadia MK, Westheimer G, Gilbert CD. Spatial distribution of contextual interactions in primary visual cortex and in visual perception. *J Neurophysiol* 84: 2048–2062, 2000.

Kato H, Bishop PO, Orban GA. Hypercomplex and simple/complex cell classifications in cat striate cortex. *J Neurophysiol* 41: 1071–1095, 1978.

Knierim JJ, van Essen DC. Neuronal responses to static texture patterns in area V1 of the alert macaque monkey. *J Neurophysiol* 67: 961–980, 1992.

Ko H, Cossell L, Baragli C, Antolik J, Clopath C, Hofer SB, Mrsic-Flogel TD. The emergence of functional microcircuits in visual cortex. *Nature* 496: 96–100, 2013. doi:10.1038/nature12015.

Ko H, Hofer SB, Pichler B, Buchanan KA, Sjöström PJ, Mrsic-Flogel TD. Functional specificity of local synaptic connections in neocortical networks. *Nature* 473: 87–91, 2011. doi:10.1038/nature09880.

Kuhlman SJ, Olivas ND, Tring E, Ikrar T, Xu X, Trachtenberg JT. A disinhibitory microcircuit initiates critical-period plasticity in the visual cortex. *Nature* 501: 543–546, 2013. doi:10.1038/nature12485.

Kuhlman SJ, Tring E, Trachtenberg JT. Fast-spiking interneurons have an initial orientation bias that is lost with vision. *Nat Neurosci* 14: 1121–1123, 2011. doi:10.1038/nn.2890.

Levitt JB, Lund JS. Contrast dependence of contextual effects in primate visual cortex. *Nature* 387: 73–76, 1997. doi:10.1038/387073a0.

Li W, Piëch V, Gilbert CD. Contour saliency in primary visual cortex. *Neuron* 50: 951–962, 2006. doi:10.1016/j.neuron.2006.04.035.

Lorenceau J, Shiffrar M, Wells N, Castet E. Different motion sensitive units are involved in recovering the direction of moving lines. *Vision Res* 33: 1207–1217, 1993. doi:10.1016/0042-6989(93)90209-F.

Maffei L, Fiorentini A. The unresponsive regions of visual cortical receptive fields. *Vision Res* 16: 1131–1139, 1976. doi:10.1016/0042-6989(76)90253-4.

Nauhaus I, Nielsen KJ, Callaway EM. Nonlinearity of two-photon Ca^{2+} imaging yields distorted measurements of tuning for V1 neuronal populations. *J Neurophysiol* 107: 923–936, 2012. doi:10.1152/jn.00725.2011.

Nelson JI, Frost BJ. Orientation-selective inhibition from beyond the classic visual receptive field. *Brain Res* 139: 359–365, 1978. doi:10.1016/0006-8993(78)90937-X.

Niell CM, Stryker MP. Highly selective receptive fields in mouse visual cortex. *J Neurosci* 28: 7520–7536, 2008. doi:10.1523/JNEUROSCI.0623-08.2008.

Nienborg H, Hasenstaub A, Nauhaus I, Taniguchi H, Huang ZJ, Callaway EM. Contrast dependence and differential contributions from somatostatin- and parvalbumin-expressing neurons to spatial integration in mouse V1. *J Neurosci* 33: 11145–11154, 2013. doi:10.1523/JNEUROSCI.5320-12.2013.

Nurminen L, Angelucci A. Multiple components of surround modulation in primary visual cortex: multiple neural circuits with multiple functions? *Vision Res* 104: 47–56, 2014. doi:10.1016/j.visres.2014.08.018.

Pack CC, Livingstone MS, Duffy KR, Born RT. End-stopping and the aperture problem: two-dimensional motion signals in macaque V1. *Neuron* 39: 671–680, 2003. doi:10.1016/S0896-6273(03)00439-2.

Pafundo DE, Nicholas MA, Zhang R, Kuhlman SJ. Top-down-mediated facilitation in the visual cortex is gated by subcortical neuromodulation. *J Neurosci* 36: 2904–2914, 2016. doi:10.1523/JNEUROSCI.2909-15.2016.

Polat U, Mizobe K, Pettet MW, Kasamatsu T, Norcia AM. Collinear stimuli regulate visual responses depending on cell's contrast threshold. *Nature* 391: 580–584, 1998. doi:10.1038/35372.

Polat U, Sagi D. Lateral interactions between spatial channels: suppression and facilitation revealed by lateral masking experiments. *Vision Res* 33: 993–999, 1993. doi:10.1016/0042-6989(93)90081-7.

Pologruto TA, Sabatini BL, Svoboda K. ScanImage: flexible software for operating laser scanning microscopes. *Biomed Eng Online* 2: 13, 2003. doi:10.1186/1475-925X-2-13.

Poort J, Khan AG, Pachitariu M, Nemri A, Orsolic I, Krupic J, Bauza M, Sahani M, Keller GB, Mrsic-Flogel TD, Hofer SB. Learning enhances sensory and multiple non-sensory representations in primary visual cortex. *Neuron* 86: 1478–1490, 2015. doi:10.1016/j.neuron.2015.05.037.

Rao RP, Ballard DH. Predictive coding in the visual cortex: a functional interpretation of some extra-classical receptive-field effects. *Nat Neurosci* 2: 79–87, 1999. doi:10.1038/4580.

Ringach DL, Shapley RM, Hawken MJ. Orientation selectivity in macaque V1: diversity and laminar dependence. *J Neurosci* 22: 5639–5651, 2002.

Rose D. Responses of single units in cat visual cortex to moving bars of light as a function of bar length. *J Physiol* 271: 1–23, 1977. doi:10.1113/jphysiol.1977.sp011987.

Roth MM, Dahmen JC, Muir DR, Imhof F, Martini FJ, Hofer SB. Thalamic nuclei convey diverse contextual information to layer 1 of visual cortex. *Nat Neurosci* 19: 299–307, 2016. doi:10.1038/nn.4197.

Rubin N, Solomon S, Hochstein S. Restricted ability to recover three-dimensional global motion from one-dimensional local signals: theoretical observations. *Vision Res* 35: 569–578, 1995. doi:10.1016/0042-6989(94)00136-A.

Sceniak MP, Hawken MJ, Shapley R. Visual spatial characterization of macaque V1 neurons. *J Neurophysiol* 85: 1873–1887, 2001.

Sceniak MP, Ringach DL, Hawken MJ, Shapley R. Contrast's effect on spatial summation by macaque V1 neurons. *Nat Neurosci* 2: 733–739, 1999. doi:10.1038/11197.

Scholl B, Pattadkal JJ, Dilly GA, Priebe NJ, Zemelman BV. Local integration accounts for weak selectivity of mouse neocortical parvalbumin interneurons. *Neuron* 87: 424–436, 2015. doi:10.1016/j.neuron.2015.06.030.

Scholl B, Tan AYY, Corey J, Priebe NJ. Emergence of orientation selectivity in the Mammalian visual pathway. *J Neurosci* 33: 10616–10624, 2013. doi:10.1523/JNEUROSCI.0404-13.2013.

Schwabe L, Ichida JM, Shushruth S, Mangapathy P, Angelucci A. Contrast-dependence of surround suppression in macaque V1: experimental testing of a recurrent network model. *Neuroimage* 52: 777–792, 2010. doi:10.1016/j.neuroimage.2010.01.032.

Self MW, Lorteije JA, Vangeneugden J, van Beest EH, Grigore ME, Levelt CN, Heimel JA, Roelfsema PR. Orientation-tuned surround suppression in mouse visual cortex. *J Neurosci* 34: 9290–9304, 2014. doi:10.1523/JNEUROSCI.5051-13.2014.

Seriès P, Lorenceau J, Frégnac Y. The "silent" surround of V1 receptive fields: theory and experiments. *J Physiol Paris* 97: 453–474, 2003. doi:10.1016/j.jphysparis.2004.01.023.

Shushruth S, Ichida JM, Levitt JB, Angelucci A. Comparison of spatial summation properties of neurons in macaque V1 and V2. *J Neurophysiol* 102: 2069–2083, 2009. doi:10.1152/jn.00512.2009.

Skottun BC. A model for end-stopping in the visual cortex. *Vision Res* 38: 2023–2035, 1998. doi:10.1016/S0042-6989(97)00293-9.

Skottun BC. End-stopping in the visual cortex: excitation or inhibition? *J Integr Neurosci* 4: 283–289, 2005. doi:10.1142/S0219635205000823.

Spratling MW. Predictive coding as a model of response properties in cortical area V1. *J Neurosci* 30: 3531–3543, 2010. doi:10.1523/JNEUROSCI.4911-09.2010.

Tan AY, Brown BD, Scholl B, Mohanty D, Priebe NJ. Orientation selectivity of synaptic input to neurons in mouse and cat primary visual cortex. *J Neurosci* 31: 12339–12350, 2011. doi:10.1523/JNEUROSCI.2039-11.2011.

von der Heydt R, Peterhans E, Dürsteler MR. Periodic-pattern-selective cells in monkey visual cortex. *J Neurosci* 12: 1416–1434, 1992.

Webb BS, Dhruv NT, Solomon SG, Tailby C, Lennie P. Early and late mechanisms of surround suppression in striate cortex of macaque. *J Neurosci* 25: 11666–11675, 2005. doi:10.1523/JNEUROSCI.3414-05.2005.

Wilson NR, Runyan CA, Wang FL, Sur M. Division and subtraction by distinct cortical inhibitory networks in vivo. *Nature* 488: 343–348, 2012. doi:10.1038/nature11347.

Xing D, Shapley RM, Hawken MJ, Ringach DL. Effect of stimulus size on the dynamics of orientation selectivity in Macaque V1. *J Neurophysiol* 94: 799–812, 2005. doi:10.1152/jn.01139.2004.

Yazdanbakhsh A, Livingstone MS. End stopping in V1 is sensitive to contrast. *Nat Neurosci* 9: 697–702, 2006. doi:10.1038/nn1693.

Yoshida T, Ozawa K, Tanaka S. Sensitivity profile for orientation selectivity in the visual cortex of goggle-reared mice. *PLoS One* 7: e40630, 2012. doi:10.1371/journal.pone.0040630.

Zhang S, Xu M, Kamigaki T, Hoang Do JP, Chang WC, Jenvay S, Miyamichi K, Luo L, Dan Y. Long-range and local circuits for top-down modulation of visual cortex processing. *Science* 345: 660–665, 2014. doi:10.1126/science.1254126.